Engineering Structures 290 (2023) 116361

Contents lists available at ScienceDirect

Engineering Structures

journal homepage: www.elsevier.com/locate/engstruct

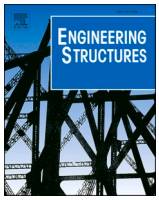

Experiment study on reactive powder concrete beams using spirals reinforcement under torsion

Xia Cao [a], Yong-peng Quan [a], Yi-cheng Ren [b], Feng Fu [c,*], Qi-zhi Jin [a,*], Da-bo He [d], Yan Zheng [a]

[a] Guangxi Key Laboratory of Green Building Materials and Construction Industrialization, Guilin University of Technology, Guilin 541004, China
[b] Construction Institute, Guangdong Technology College, Zhaoqing 526000, China
[c] Department of Engineering, School of Science and Technology, City, University of London, EC1V,0HB, UK
[d] Construction Institute, Nanning Technology College, Guilin 541004, China

ARTICLE INFO

Keywords:
Spiral reinforcement
Reactive powder concrete beam
Torsional performance

ABSTRACT

This paper investigates the torsional behavior of reactive powder concrete (RPC) beams using spiral reinforcement. The influences of parameters, including different spiral reinforcement configuration, spiral reinforcement ratio, and the steel fiber content on the torsional performance of the nine RPC beams, were investigated and discussed. The experimental results showed that the failure mode, ultimate torque, torsional stiffness, and energy dissipation of the RPC beams were not affected by longitudinal reinforcement alone, but it improved the ductility. Compared to commonly used stirrups, the locked spiral reinforcement exhibits more torsional ductility, stiffness, and ultimate torque of the RPC beams. But the torsional ductility, stiffness, and ultimate torque decreased when the spiral reinforcement was unlocked. The cracking torque and pre-cracking torsional stiffness of beams were less affected by the locking and unlocking of spiral reinforcement. Greater steel fiber content and spiral reinforcement ratio resulted in higher torsional ductility, torsional stiffness, energy dissipation and ultimate torque of the locked spiral reinforcement reinforced beams. The pre-yielding torsional stiffness and plastic dissipation capacity were strongly influenced by spiral reinforcement states and spiral reinforcement ratio. The pre-cracking torsional stiffness and energy dissipation of RPC beam were determined by the steel fiber content. Considering the torsional contribution of steel fiber and concrete tensile strength, a new formula for calculating the ultimate torque of RPC beam was proposed, and the calculated value was closer to the experimental value.

1. Introduction

Building and bridge structures have become complex and irregular, some beams subject to large torques, such as border beams, canopy beams, and curved bridges. In this case, the beams need to have high torsional capacity and ductility, especially in typhoon or earthquake-prone areas, which poses new challenges to the torsional performance of the beam [1–3]. In recent years, the advantages of using continuous spiral reinforcement (SP) instead of ordinary stirrups have been recognized in terms of improving the capacity and ductility of members. The application of SP significantly improves the shear performance of beams, energy dissipation and deformation capacity of beam-column joints, and the bearing capacity and seismic performance of shear walls [4–8]. Therefore, research relating to the use of SP in torsional beams has been gradually carried out.

Shatarat et al.[9] designed beams with three types of spiral reinforcement and investigated the effect of spiral reinforcement form on the torsional capacity of beams. The results showed that the continuous circular spiral stirrup had the largest enhancement in ultimate torque, followed by the continuous SP, and finally the advanced rectangular spiral reinforcement and the ordinary stirrups. However, circular spiral stirrups were seldom used in beams, while rectangular spiral reinforcement were paid more attention by researchers. Chalioris et al.[10] investigated the locking and unlocking effect on the torsional capacity and ductility of beams, and the results indicated that locked SP significantly improved the torsional capacity and ductility of beams. This is consistent with the conclusions from Ibrahim et al [11]. The torsional capacity and ductility decreased significantly, when the SP was unlocked. Shahrooz et al.[12] pointed out experimentally that the torque of test beams with SP was subjected should be lower than the cracking torque, when the direction of the torque was uncertain. In addition, the locking and unlocking effect of spiral reinforcement usually occurs in the column due to the action of cyclic torque [13–15].

* Corresponding authors.
E-mail addresses: feng.fu.1@city.ac.uk (F. Fu), 2014056@glut.edu.cn (Q.-z. Jin).

https://doi.org/10.1016/j.engstruct.2023.116361
Received 9 February 2023; Received in revised form 21 April 2023; Accepted 18 May 2023
Available online 28 May 2023

Nomenclature

Notation

d_f	diameter of fiber,mm
l_f	length of fiber,mm
f_t	tensile strength of fiber,MPa
$f_{c,m}$	cubic compressive strength of RPC,MPa
$f_{t,m}$	tensile strength of RPC, MPa.
ξ_θ	ultimate-to-cracking twist ratio
θ_u	ultimate twist,rad/m; θ_{cr} cracking twist,rad/m
K_{cr}	the pre-cracking torsional stiffness,kN·m^2/rad
K_y	the pre-yielding torsional stiffness,kN·m^2/rad
K_u	the pre- ultimate torsional stiffness,kN·m^2/rad
W	total energy dissipation of tested beam,kN·m^2
W_E	the elastic deformation energy dissipation,kN·m^2
W_P	the plastic deformation energy dissipation,kN·m^2
V_f	The total volume of steel fibers,%
A_{SF}	steel fiber equivalent stirrups with cross-sectional area,mm^2
b,h	the width and height of tested beam,mm
b_0,h_0	the width and height of the area enclosed by the centerline of the stirrup,mm
S	the stirrup spacing of tested beam,mm
A_{LR}	the cross-sectional area of all longitudinal reinforcements,mm^2
f_{LR}	the yield strength of the longitudinal reinforcement,MPa
A_{TR}	the cross-sectional area of single transverse reinforcement,mm^2
f_{TR}	the yield strength of the transverse reinforcement,MPa
$\varphi_{fornt},\varphi_{top}$	the inclination angles of the side and top of spiral reinforcement
T_{cr}	measured torsional moment at cracking,kN·m
T_y	measured torsional moment at stirrup yielding,kN·m
T_u	measured ultimate torsional moment,kN·m
T_{cal}	calculated ultimate torsional moment,kN·m

However, the direction of the torque born by the beam is basically determined, so the beam with SP still has greater application value. Therefore, Hadhood et al.[16] further investigated the effect of SP spacing on the torsional performance of beams. It was proved that the stiffness and ultimate torque of the beams decreased with the increase of stirrup spacing.

At the same time, a limitation of the SP was exposed, which could not effectively improve the cracking torque of the beams [9–10]. The appearance of torsional cracks reduced the torsional performance and durability.[17–19]. Compared to regular concrete, RPC has higher tensile strength and durability, which improves the cracking load of the members [20–21]. Khuzaie et al.[22] carried out torsional tests on hollow RPC T-beams. The results illustrated that the cracking torque of the beams was improved and the development of cracks was retarded. Yang et al.[23] and Zhou et al.[24] experimentally demonstrated that the cracking torque and ultimate torque of ultra-high performance concrete (UHPC) beams increased with the increase of steel fibers content. Kwahk et al.[25]conducted pure torsion tests on UHPC box beams and found that the influence of steel fiber on cracking torque was greater than that of stirrups.

In summary, RPC significantly increases the cracking torque of beams, and compensates for the defects in the unlocking effect of SP. It is predictable that the beams with combination of the SP and RPC can improve torsion performance. However, there is a little research on the torsional performance of RPC beams with SP, and the working mechanism and related theories of both are still unclear. With this problem in mind, the study aims to investigate the torsional behavior of RPC beams with SP. The nine RPC beams were fabricated and tested. The effect of different spiral reinforcement states, spiral reinforcement ratio, and steel fibers content on the torsional performance of RPC beams was studied. It can provide a guideline for the engineering application of RPC beams with SP.

2. Experimental program

2.1. Properties of materials

The materials used to prepare RPC include cement (PO42.5), silica fume, silica sand, superplasticizer, water and steel fiber. The mix design and mechanical properties of RPC are shown in Table 1 and Table 2, respectively. There were three RPC mixtures used in this experiment, and only the steel fiber content was different. To prepare RPC, silica sand with three different diameter first were put into a mixer for 2 min. Secondly, the steel fibers were added to the mixer by steel sieve, and continued to mix for 2 min. Thirdly, silica fume and cement were poured in the mixture when the steel fibers were dispersed and stirred for 10 min. Finally, water-reducing admixture and water were dropped sequentially and mixed for 6 min to obtain RPC with high fluidity and usability [26–27]. The test beams and cube specimen were concreted at the same time and consistently maintained in the same environment. The compressive and tensile strengths of RPC were measured from cubic specimens, as shown in Table 3. The longitudinal and transverse reinforcements were HRB400 steel reinforcements. The SP was made from whole continuous rebars. The properties of used rebars are presented in Table 4.

Table 2
Material properties.

Materials	property
cement	PO42.5 portland cement, specific surface area 360 mm^2/kg
silica sand	the particle size of coarse, medium and fine sand is 0.16–0.315 mm, 0.315–0.63 mm, 0.63–1.25 mm.
Silica fume	the silica content is 92%, average particle size is 0.3 μm
Steel fibers	straight steel fiber, d_f is 0.22 mm, l_f is 13 mm, f_t is 2000 MPa
Super-plasticizer	MKM-1021 Superplasticizer, white powder, Water reduction rate 29%

Whered_f = diameter of fiber, l_f= length of fiber, f_t=tensile strength of fiber.

Table 1
Mix design of RPC.

Cement	Silica sand			Silica fume	Steel fibers	Super-plasticizer	Water
	Coarse	Medium	Fine				
1	0.2	0.8	0.2	0.3	0.75%/1.5%/3%	0.02	0.23

Where: steel fiber is the volume dose.

Table 3
Mechanical properties of RPC.

Steel fiber content	Number of cubes	$f_{c,m}$(MPa)	$f_{t,m}$(MPa)
0.75%	6	116.2	4.2
1.5%	6	123.8	6.6
3%	6	131.6	7.9

Where$f_{c,m}$ = cubic compressive strength of RPC, $f_{t,m}$=tensile strength of RPC.

Table 4
Mechanical properties of steel rebar.

Types	Function	d(mm)	f_y(MPa)	f_u(MPa)	E(GPa)
HRB400	stirrup	10	452	603	200
	Longitudinal rebar	12	467	611	200

Where$d$ = diameter of rebar, f_y= yield strength of steel rebar, f_u= ultimate strength of rebar, E= elastic modulus of rebar.

2.2. Details of test specimen

Nine rectangular RPC beams were designed with length of 2100 mm and cross section dimension of 150 × 250 mm^2. Each beam was divided into two zones: pure torsion test region (1200 mm) and support region (900mm), as shown in Fig. 1. To ensure damage in the pure torsion test region, ordinary stirrup with spacing of 50 mm was used in the support region. The main design parameters of the test beam are provided in Table 5. "ST'' for the ordinary stirrups, "SP'' for the rectangular spiral reinforcement, and details of the SP are shown in Fig. 2 "L'' for the beams with SP under beneficially implemented action of the torsional direction that leaded spirals to be locked, "U'' for the beams with SP under detrimentally implemented action of the torsional direction that lead spirals to be unlocked [10]. The RPC beams without longitudinal and transverse reinforcement and with only longitudinal reinforcement were denoted by "P" and "I", respectively. The designation of the test beams with transverse reinforcement was comprised of its own primary parameters. The order of designation was ST/SP-100/150/200-U/L-0.75/1.50/3.00. For example, SP-100-L-0.75 represents a RPC beam with spiral reinforcement (SP), stirrup spacing of 100 mm (100), spiral reinforcement locked in the direction of torque loading (L), and steel fiber content of 0.75% (0.75).

2.3. Test setup and procedure

The test setup was assembled according to Shatarat and Chalioris [9–10], as shown in Fig. 3. The test pricedure also refer to [40–42] when designing it. The concentrated force exerted by the hydraulic jack was transferred to the steel cross beam (length of 0.61 mm) through the steel distribution beam (length of 3.00 mm). The hydraulic jack was bolted to the steel distribution beam to ensure the safety of test process. Then, the concentrated forces withstand by the steel cross beam was transformed into torque at the ends of the beam. The balance plates could be balanced or rotated freely by adjusting the balance bolt and were placed

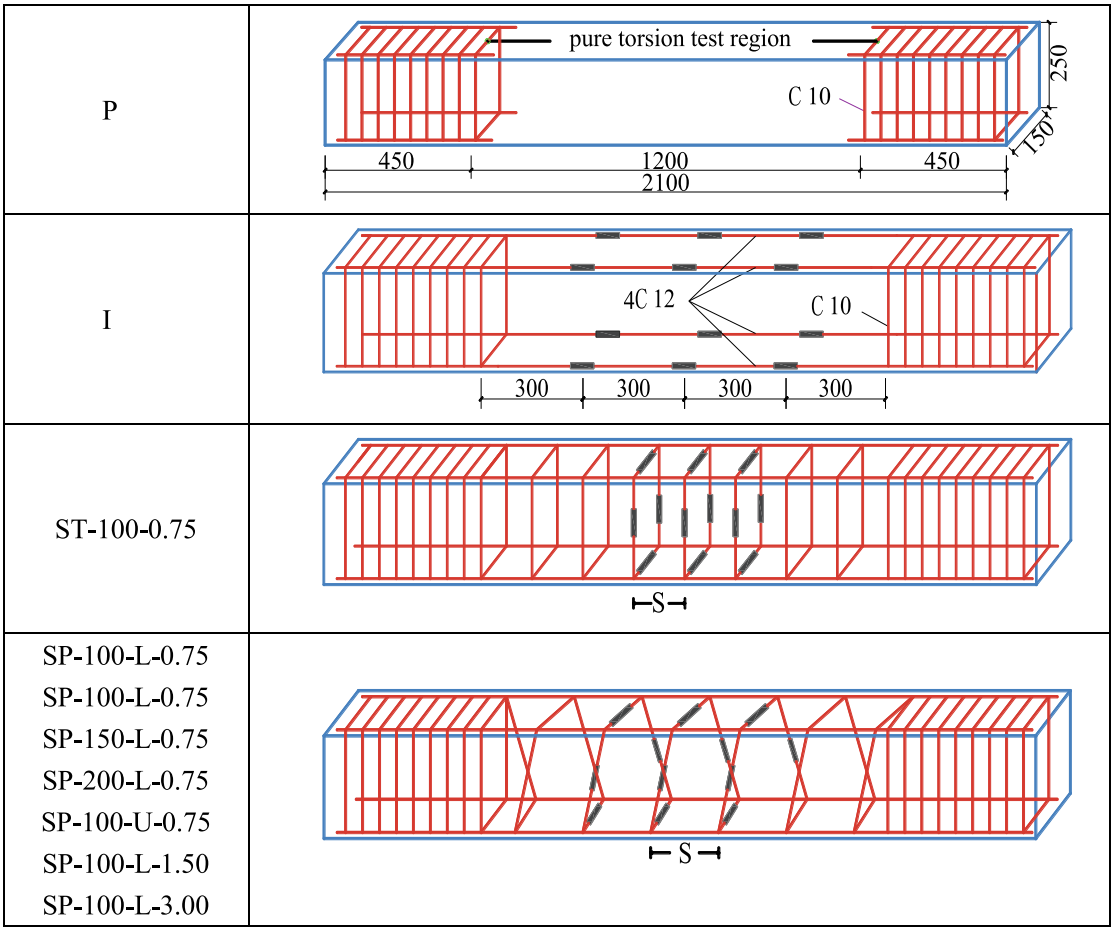

Fig. 1. Details of test beams.

Table 5
Main parameters of RPC beams.

Test beam	ρ_l(%)	ρ_t(%)	φ(°)	Stirrup types	Stirrup spacing (mm)	Torque direction	Steel fiber content
P	–	–					0.75%
I	1.206	–					0.75%
ST-100–0.75	1.206	1.340		ST	100		0.75%
SP-100-L-0.75	1.206	1.356	81	SP	100	L	0.75%
SP-100-U-0.75	1.206	1.356	81	SP	100	U	0.75%
SP-150-L-0.75	1.206	0.917	77	SP	150	L	0.75%
SP-200-L-0.75	1.206	0.700	73	SP	200	L	0.75%
SP-100-L-1.50	1.206	1.356	58	SP	100	L	1.50%
SP-100-L-3.00	1.206	1.356	58	SP	100	L	3.00%

Whereρ_l = longitudinal reinforcement ratio, ρ_t=stirrup ratio, φ= inclination angle between stirrup and the longitudinal axis of the beam, as shown in Fig. 2.

in two roller supports 1150 mm apart.

The test was conducted by graded loads, as presented in Fig. 4. The cracking and ultimate torque (T_{cr} and T_u) of RPC beams were predicted according to the equations in ACI 318–19 [28]. Before reaching the estimated cracking torque, each load increment was 2 kN, and each load increment was 1 kN when approaching the estimated cracking torque. After the tested beam was cracked, each load increment continued to be 2kN, and each load increment was 1kN when the predicted ultimate torque was approached. The load of each increment was maintained for 5 min in order to record all crucial test data.

Strain gages were attached at the longitudinal or transverse reinforcement (Fig. 1) to measure the strains in the rebar. Concrete strain gauges and digital inclinometers were respectively arranged at the quarter point on side and top of pure torsion test region to measure concrete strain and torsional angle, as depicted in Fig. 3. The cracks width on the surface of the beam was recorded using a crack observer with an accuracy of 0.02 mm under each load increment. After the test beam failed, the angle of the main crack inclination was measured using a high precision digital display angle scale.

3. Experimental results and discussion

The characteristic loads and failure modes of the test beams are given in Table 6. Each characteristic load had included the self-weight of the steel beam in the test setup. To compare the characteristic loads of the beams, the torque at the appearance of the first visible crack was defined as the cracking torque, and the torque at the yielding of the stirrup was the yielding torque. When the stirrup was not yielded, yielding torque could be taken as 0.8 T_u. The failure mode is considered based on the observation of the actual failure and the strain of the reinforcement in each beam.

3.1. Cracking patterns and failure modes

3.1.1. Cracking patterns

The cracking development process of P and I was similar. After the first crack appeared, the crack width increased rapidly until the beam was damaged. The crack process of RPC beams with stirrups was less affected by different spiral reinforcement states, spiral reinforcement ratio, and the steel fiber content. As an example, the crack process of ST-100–0.75 was documented, as seen in Fig. 5. When reached the cracking torque, the first visible diagonal crack with a distinct sound was found on the side of the beam. New diagonal cracks appeared continuously and the inclination of the new cracks remains unchanged practically with the increase of the torque. Many diagonal cracks had extended to the top and bottom, forming spiral cracks on the surface of the beam at a torque of 0.5 T_u. New diagonal cracks hardly appeared, and the previous crack width increased at a torque of 0.8 T_u. After the torque was approximately 0.9 T_u, the main crack appeared and increased with the increase of torsional angles until the beam was damaged. Moreover, there was no large concrete falling off due to the existence of steel fiber when the beam was damaged. This phenomenon was different from ordinary concrete beams [29–30].

3.1.2. Failure modes

The cracks pattern and failure modes of RPC beams are provided in Fig. 6. There was only a single helical crack of large width on the surface of the beam when P and L were damaged. The failure process was rapid and brittle, and P was suddenly divided into two parts while L did not fracture due to the presence of longitudinal reinforcement. It shows that the longitudinal reinforcement only had little effect on limiting the cracks and could not change the failure mode, which was consistent with the results of ordinary concrete beams [31–32]. For RPC beams with SP, the locking and unlocking of SP could cause changes in failure modes, while the spiral reinforcement ratio and steel fiber content had less effect. When the test beam was damaged, the stirrups and longitudinal bars of SP-100-L-0.75 yielded. Only the longitudinal bars yielded when SP-100-U-0.75 was damaged because the SP were unlocked. Compared to beams without stirrups, the presence of stirrups increased the torsional deformation and ductility of SP-100-L-0.75 and SP-100-L-0.75. But the failure process of SP-100-U-0.75 was faster and had a certain brittleness. Because the damage of SP-100-U-0.75 was determined by the concrete, the tensile properties of the steel rebars were not fully utilized. When the SP was locked, the increasing spiral reinforcement ratio and steel fibers effectively inhibited the development of cracks and improved the deformation capacity of the tested beam. Therefore, the failure of SP-100/150/200-L-0.75 and SP-100-L-1.50/3.00 were ductile failures. This is attributed to that longitudinal rebars, and stirrups had yielded before the concrete was crushed, and the tensile properties of the bars were fully utilized.

The main diagonal cracks angle is also marked in Fig. 6. The main crack inclination angle was influenced by the test parameters. The reason is that crack angle depends on the direction of the main tensile stress which is related to the stress state of the stirrups and steel fibers. Meanwhile, it is observed that SP-100-L-0.75 exhibited more fine cracks than ST-100–0.75 and the opposite phenomenon was found in SP-100-U-0.75. And the number of fine cracks increases with the decrease of stirrup spacing or the increase of steel fiber content. This indicates that both spiral reinforcement and steel fibers could promote multiple cracking and stress redistribution ability of RPC beams. The excellent characteristic was greatly weakened when the SP was unlocked or the stirrup spacing was increased. However, the excellent characteristic was further enhanced when the steel fiber content was increased.

3.2. Torque – Rebar strain relationships

Fig. 7 shows the torque versus strain curves of longitudinal rebar and stirrup at the midspan of each RPC beam. The maximum strain of longitudinal reinforcement of I was 800 × 10^{-6}με, which was much smaller than that of RPC beams with stirrups. It shows that longitudinal rebars hardly bore the tensile stresses due to the torque. The variation of rebar strain with torque for the other beam was basically similar. Before

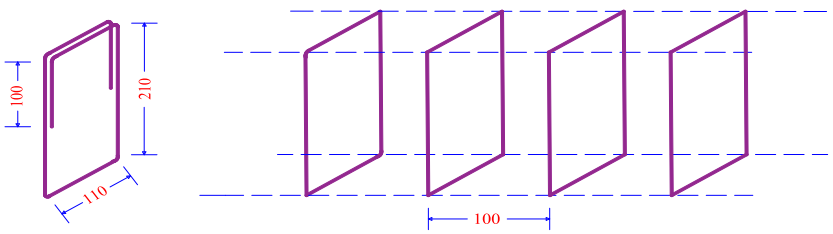

Ordinary stirrup with stirrup spacing of 100mm

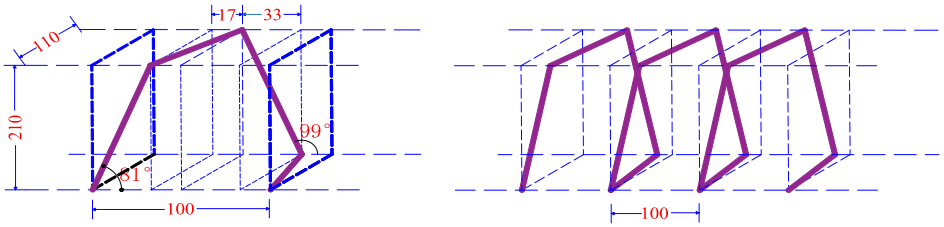

The SP with spacing of 100mm

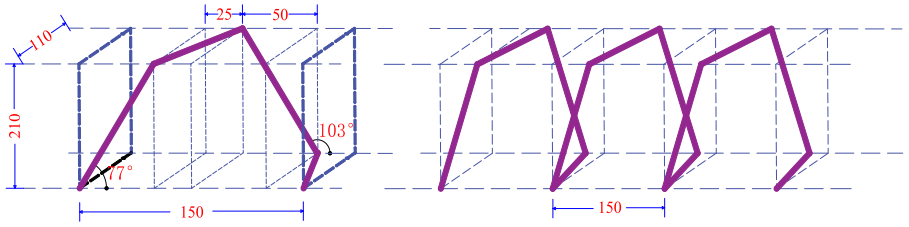

The SP with spacing of 150mm

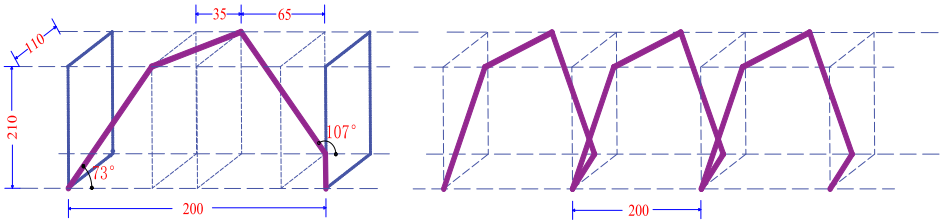

The SP with spacing of 200mm

2(a)

2(b)

Fig. 2. Details of stirrups, (a) schematic stirrups, (b) actual stirrups.

cracking, the strain growth of longitudinal rebar and stirrup was small and linear. The strain on both started to increase rapidly after the first crack was discovered. After cracking, the torque was jointly borne by the whole formed by the concrete, steel bars and steel fibers. In this case, the concrete was under compression and the steel bars or steel fibers were under tension. Therefore, the reinforcement intersecting the diagonal crack was subjected to higher tensile forces during cracking. This results in a flat section in the torque versus curve.

Compared to SP-100-L-0.75, SP-100-L-1.50 and SP-100-L-3.00 had shorter flat sections, while ST-100–0.75 and SP-100-U-0.75 basically had no flat sections. This phenomenon reveals that the locked SP effectively withstood the tensile forces in the beam after cracking due to the superb ability of capturing cracks. But the unlocked SP bore less tension due to the stirrup being parallel to the crack. Moreover, the steel

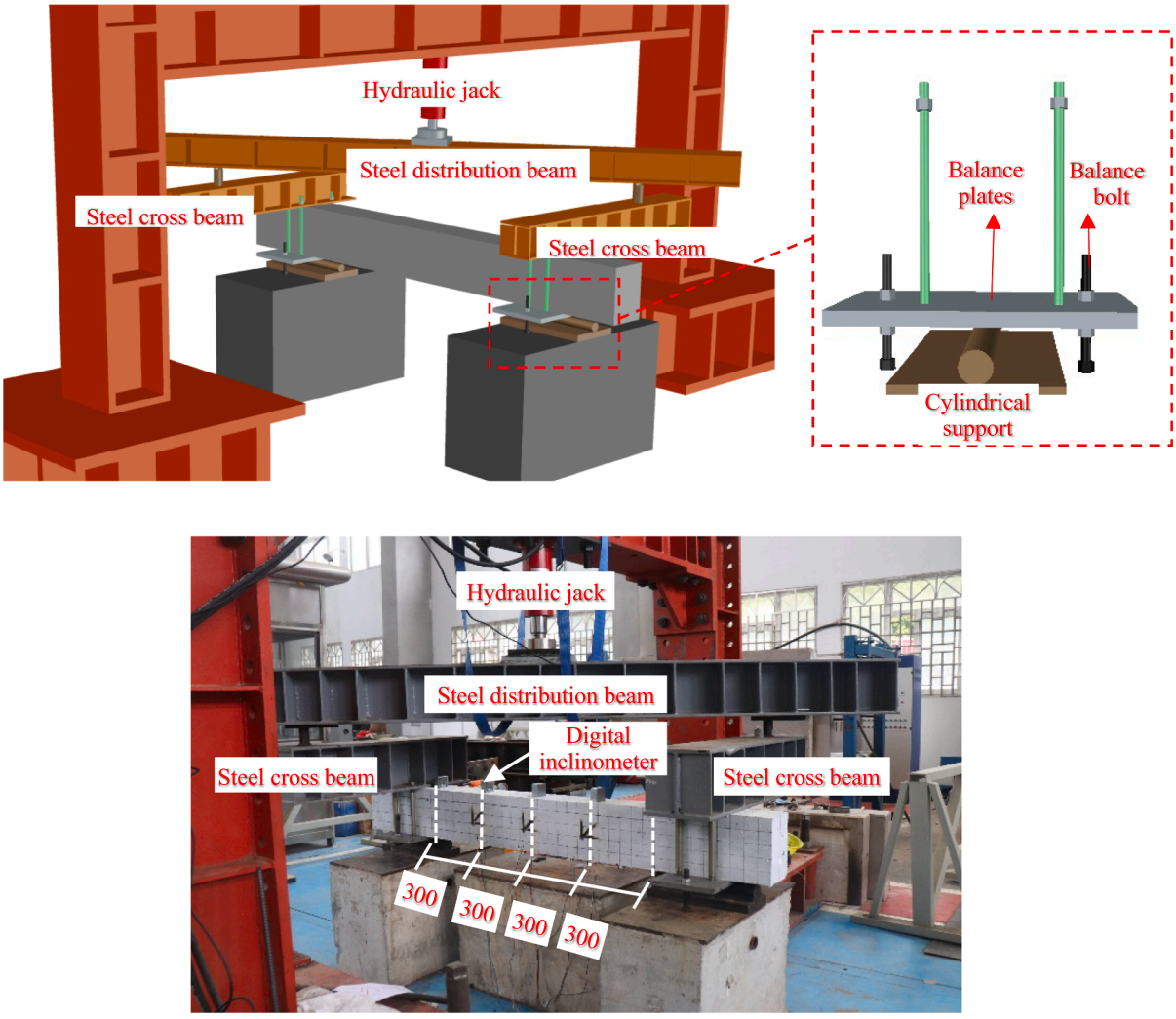

Fig. 3. Details of test setup, (a) schematic test setup, (b) actual test setup.

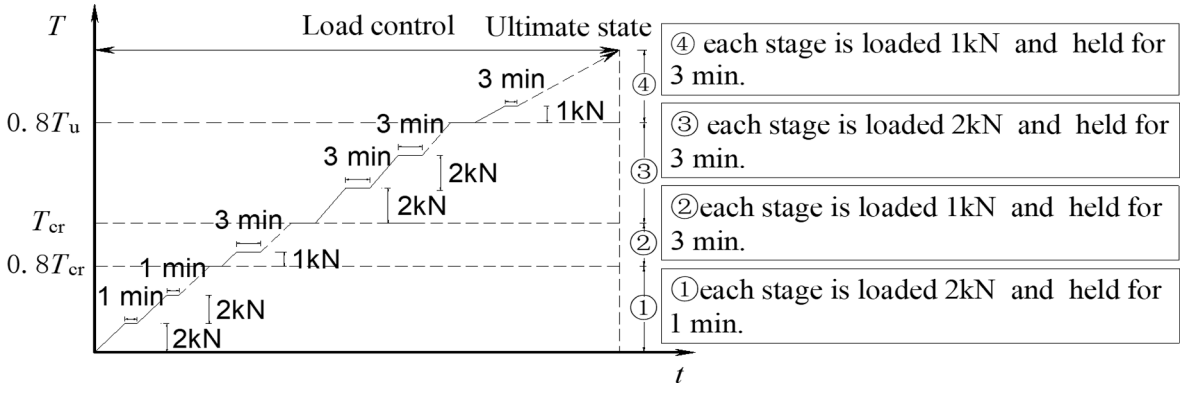

Fig. 4. Load control.

fiber significantly shared the tensile force of the stirrup, and better restrained the sudden increase of the stirrup strain.

The maximum strain of longitudinal rebar and stirrup for ST-100–0.75 was only 2575 $\times$ 10^{-6}με, yet the minimum strain of SP-100-L-0.75 reached 5000 $\times$ 10^{-6}με. This means that the synergy between locked SP and longitudinal bars was better than that of ordinary stirrup. Therefore, the beneficial tensile properties of the SP were fully used, in agreement with previous study [16]. However, the SP was more likely to yield with increasing the spacing of stirrup, and longitudinal strain was reduced. This means that the synergy between steel bars was weakened as the spacing of SP widened. It is worth noting that the synergy between the unlocked SP and longitudinal reinforcement was the worst, and the effect of the steel fiber on the synergy was small.

Table 6
Characteristic loads and failure modes of RPC beams.

Test beam	Cracking point		Yield point		Ultimate Point		Failure mode
	T_{cr} (kN·m)	θ_{cr} (rad/m)	T_y (kN·m)	θ_y (rad/m)	T_u (kN·m)	θ_u (rad/m)	
P	7.93	0.0021	—	—	7.93	0.0021	CF
I	7.82	0.0025	—	—	8.43	0.0042	CF
ST-100–0.75	8.52	0.0034	14.40	0.0295	18.27	0.0735	CFSY
SP-100-L-0.75	8.48	0.0029	16.20	0.0298	20.45	0.0844	CFSY
SP-100-U-0.75	8.38	0.0019	12.30	0.0193	15.37	0.0333	CFLY
SP-150-L-0.75	7.87	0.0028	14.06	0.0342	17.32	0.0640	CFSY
SP-200-L-0.75	7.35	0.0030	11.04	0.0374	16.01	0.0575	CFSY
SP-100-L-1.50	10.5	0.0025	19.86	0.0263	23.56	0.0909	CFSY
SP-100-L-3.00	11.7	0.0029	26.02	0.0305	29.49	0.1153	CFSY

Where CF = Concrete failure, CFSY = Longitudinal reinforcement and stirrup yielded before final concrete failure, CFLY = Longitudinal reinforcement only yielded before final concrete failure.

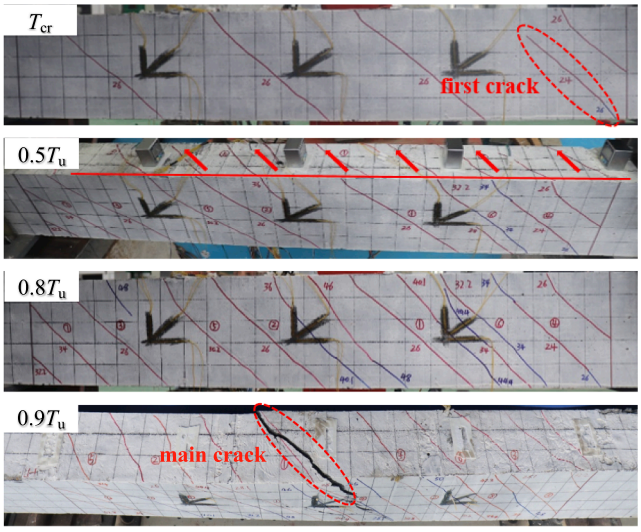

Fig. 5. Crack process of RPC beams.

3.3. Torque –maximum crack width relationships

Fig. 8 depicts the variation of torque with maximum crack width. The crack widths of P and I were not measured due to failure rapidly. Except for SP-100-U-0.75, the torque-maximum crack width curves of test beams were divided into a steady development stage and a rapid expansion stage. In the steady development stage, the crack width grew linearly and steadily with the addition of torque. Because the cracks were limited by steel fibers and stirrup in elastic phase. When approached the ultimate torque, most of the steel fibers were pulled out and the stirrup was close to yielding. Therefore, the limitation of yielded stirrup on diagonal crack was weakened and the crack width grew quickly during a rapid expansion stage.

SP-100-U-0.75 had the largest crack growth rate among all RPC beams. When the SP was unlocked, the tensile force borne by the SP was reduced because the inclination of the stirrups was parallel to the inclined cracks. Therefore, the unlocked SP had almost no limiting effect on cracks. It also is observed from the steady development stage that the duration of SP-100-L-0.75 was greater than that of ST-100–0.75. Compared with SP-100-L-0.75, the slope of curves decreased for SP-150/200-L-0.75 and SP-100-U-0.75 and increased for SP-100-L-1.50/3.00. This implies that the SP was better than normal stirrup in restraining cracks. While the spacing of SP was increased or the SP was unlocked, the restraining effect was reduced. Steel fibers shared the tensile force borne by the stirrups and enhanced the restraining effect on cracks. Besides, it is also found that the crack growth rate in the rapid expansion stage was basically not affected by the spacing of SP and steel fibers content.

3.4. Torque – twist relationships

Twist is defined as the ratio of the angular differential between the two ends of the beam to the length of the pure torsion region [33]. The measured torque versus twist curve of RPC beam is shown in Fig. 9. Before cracking, the twist increased linearly and finely. The twist was basically unaffected by spiral reinforcement states, spiral reinforcement ratio, and the steel fiber content during this period. Because the twist was mainly related to concrete before cracking. The twist of RPC beams began to increase rapidly with the appearance of cracks. The effect of spiral reinforcement states, spiral reinforcement ratio, and the steel fiber content on twist also began to appear. This implies that the twist of RPC beams with normal stirrup was significantly better than that of beams with unlocked SP, while the torsional deformation of RPC beams with locked SP was better than that of RPC beam with normal stirrup. With the increase of spiral reinforcement spacing, the twist tended to decrease. On the contrary, the addition of steel fibers significantly enhanced the twist of the beam. This is explained that twist was closely related to the synergy of longitudinal rebar and stirrup after cracking. When the beam was damaged, the synergy of steel rebar resulted in greater torsional deformation. Because the synergy between longitudinal rebars and stirrup was better, the beam still supported the torque under the condition of large torsional deformation.

4. Influence of experimental parameters on torsional behavior

4.1. Cracking torque

The cracking torque of RPC beams is summarized in Fig. 10. Compared with P and I, the cracking torque of ST-100–0.75 was increased by 6.9% and 8.2% respectively. The cracking torque of SP-100-L-0.75 was basically the same as ST-100–0.75, and SP-100-U-0.75 was similar to the RPC beams without stirrups (P and I). This proves that the form of stirrups and the unlocking and locking of SP had little effect on the cracking torque. Although the stirrups could bear the tensile force in the beam, the force before cracking was small. So, the influence of the stirrups on the cracking torque was small.

Similarly, with the increase of stirrups spacing, the force further diminished, resulting in a reduction of cracking torque of RPC beam. When the spacing of SP changed from 100 mm to 150 mm and 200 mm, the cracking torque dropped by 7.2% and 13.3% respectively. For ordinary concrete beams, when the voluminal sum of longitudinal and transverse reinforcement ratio is less than 0.014, steel rebar will have a greater effect on cracking torque. However, the influence of steel rebar on cracking torque of the beam was smaller when the total voluminal ratio was greater than 0.014. From the experimental results of Yang [23] and this paper, the RPC beam also conformed to the above law.

Contrary to the state and spacing of SP, the cracking torque was

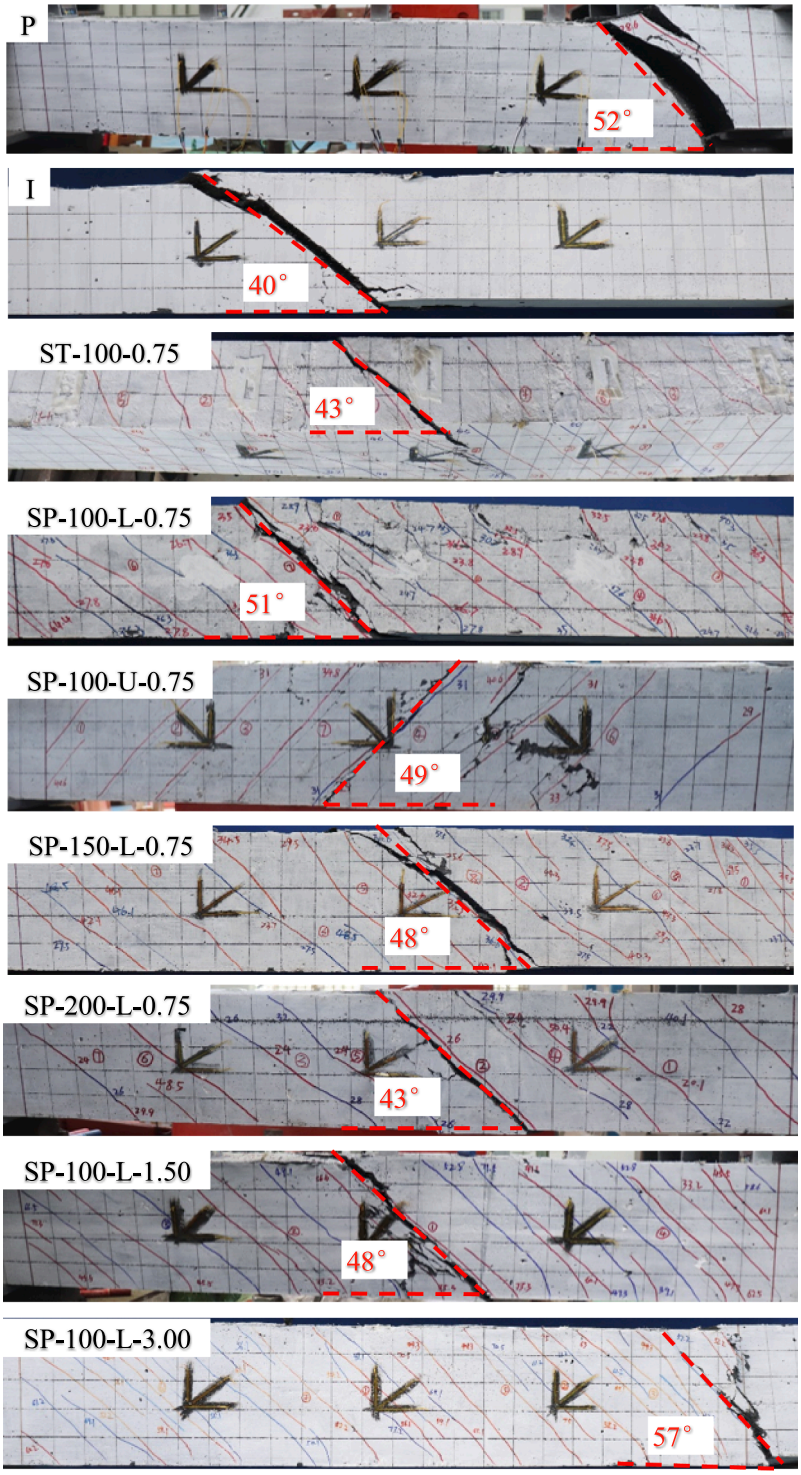

Fig. 6. Failure modes.

strongly influenced by the steel fibers, in agreement with the conclusion of Kwahk [25]. The cracking torque of SP-100-L-1.50 and SP-100-L-3.00 was 23.2% and 38% higher than that of SP-100-L-0.75, distinctly. This is revealed that the steel fiber undertook the tension in the beam through bonding effect, and hindered the crack generation. The tension was also dispersed by the steel fibers of RPC beams, avoiding the occurrence of stress concentration.

4.2. Ultimate torque

The ultimate torque of RPC beams and variation rule with the test parameters are illustrated in Fig. 11. The difference of ultimate torque between P and I was small. The use of longitudinal bars alone did not prevent the concrete from being pulled, so the ultimate torque of the beams without stirrups was slightly increased. The ultimate torque of RPC beams with stirrups varied greatly depending on unlocking and locking of SP, stirrup spacing and steel fibers content.

Compared with ST-100–0.75, the ultimate torque of SP-100-L-0.75

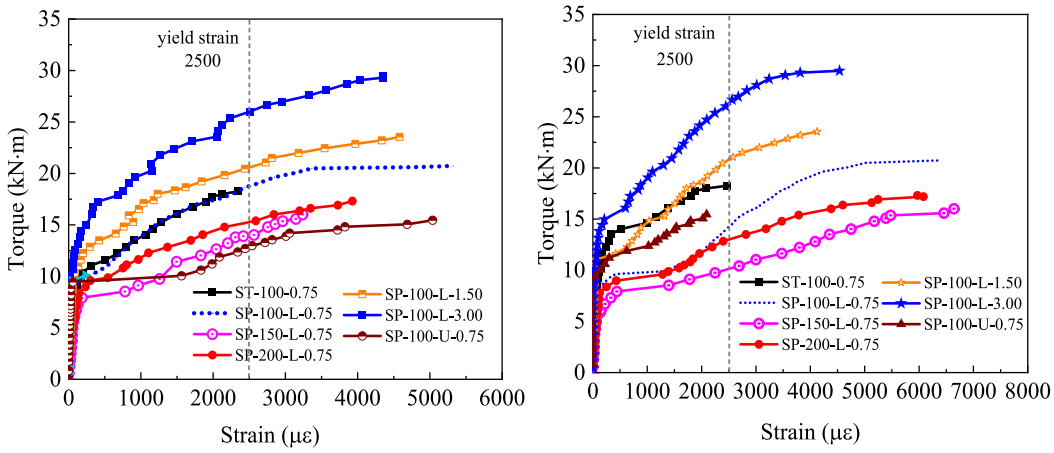

Fig. 7. Torque–rebar strain relationships, (a) Torque–longitudinal rebar strain relationships (b) Torque–transverse rebar strain relationships.

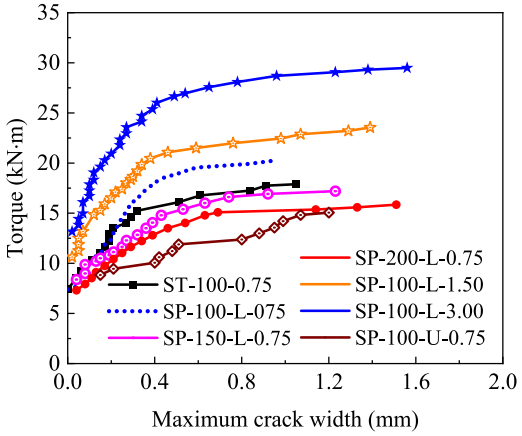

Fig. 8. Torque –maximum crack width relationships.

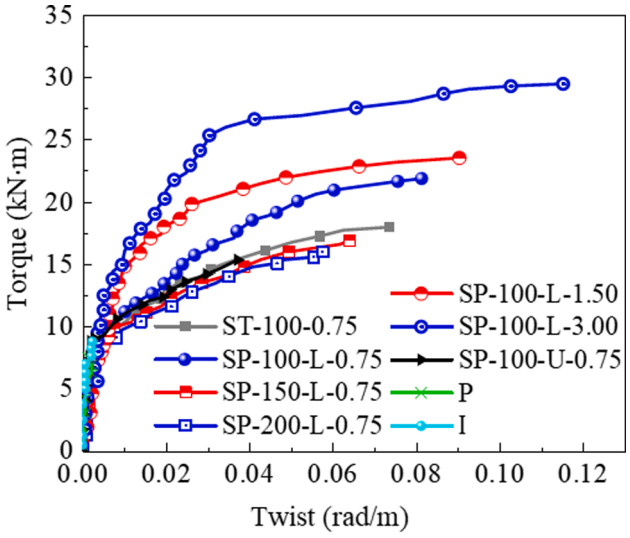

Fig. 9. Torque – twist relationships.

was increased by 11.9%, while the ultimate torque of SP-100-U-0.75 was reduced by 15.9%. The unlocking and locking effect of the SP could result in a difference of 27.8% in the ultimate torque of RPC beams. However, the unlocking and locking effect of SP leaded to an average difference of 37.1% in the ultimate torque of the ordinary concrete beam [10]. This implies that steel fibers weaken the unlocking effect of the SP and reduced the influence of the torque direction on ultimate torque of specimens. This conclusion is also proved by Shahrooz et al [12].

With increased stirrup spacing from 100 mm to 150 mm and 200 mm, the ultimate torque was reduced by 15.3% and 21.7% respectively. When the steel fiber content was added from 0.75% to 1.50% and 3.00%, the ultimate torque of SP-100-L-1.50 and SP-100-L-3.00 was increased by 15.2% and 44.2%, respectively. This implies that steel fibers had the greater influence on the ultimate torque of RPC beams with SP among the parameters and should be considered in the ultimate torque calculation equation.

The ultimate torque of RPC beams with locked SP was enhanced compared to that of the RPC beams with ordinary stirrup. After the single ordinary stirrup was yielded, it was difficult to transfer the tension to the adjacent stirrup due to the independence and non-uniformity of the force of ordinary stirrup. The tensile force was resisted by the concrete and the crack width increased rapidly, which was more likely to cause the failure of RPC beams. Difference to the ordinary stirrup, the tension borne by the locked SP was uniform and greater because of its continuity and integrity. Meanwhile, the locked SP in tension produced an approximate triaxial compression on the concrete in the core area. It provided extra constraint in concrete and the constraints was enhanced with the increase of tension. Therefore, the concrete with cracks in the late loading period was hardly subjected to tension, but still bore larger compressive stresses through the constraint. As a result, concrete with oblique cracks could form a new stress system with steel rebar to bear greater torque. However, it was basically unable to share the tensile force for the concrete when the SP was unlocked. And the unlocked SP also could not form effective restraint on the concrete in the core area, thus the ultimate torque was dramatic descended. In addition, the increase of stirrup spacing was accompanied by the decrease of the tensile force and restraint. This causes the decrease of ultimate torque when the stirrup spacing becomes wider. Contrary to the stirrup spacing, the use of steel fibers not only shared the tensile force borne by the stirrups, but also increased the tensile strength of concrete. It is a clear interpretation that the ultimate torque increased with increasing steel fiber content.

4.3. Torsional ductility

Ultimate-to-cracking twist ratio ξ_θ reflects the ductility of the tested beam, and the larger the ξ_θ resulted in better the ductility of the beams [34–35]. ξ_θ is defined as follows:

$$\xi_\theta = \frac{\theta_u}{\theta_{cr}} \tag{1}$$

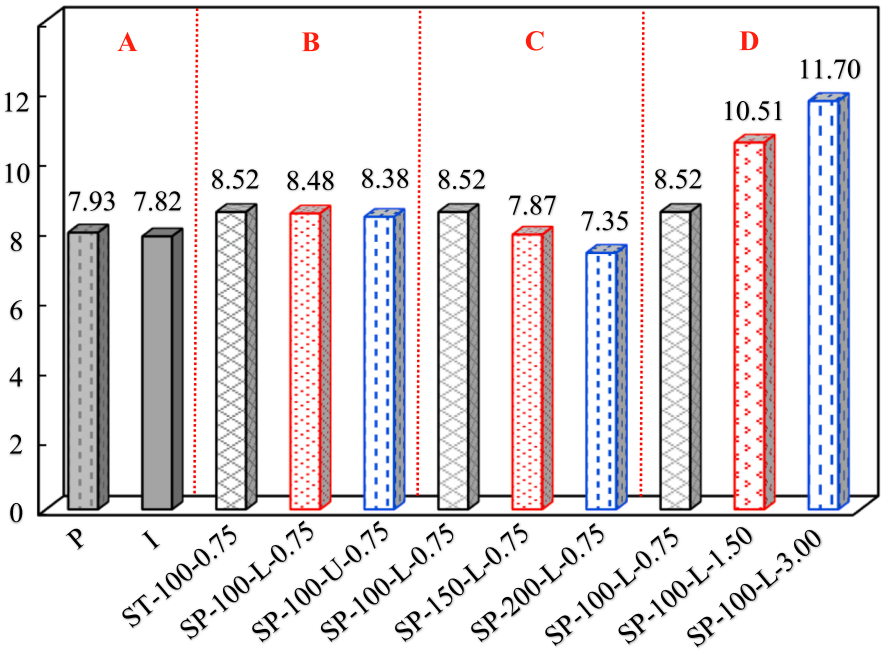

Fig. 10. Effects of test parameters on cracking torque. where A for control group, B for effect of spiral reinforcement condition on cracking torque, C for effect of spiral reinforcement spacing on cracking torque, D for effect of steel fiber content on cracking torque.

Where: θ_u is ultimate twist; θ_{cr} is cracking twist.

The values of ξ_θ for all RPC beams are summarized in Fig. 12. P and I without stirrups instantly collapsed after cracking and had the worst ductility. Under the same stirrup spacing, the ductility of RPC beam with locked SP was better than that of ordinary stirrup beam (increased by 34.6%), while RPC beam was inferior to ordinary stirrup beam (decreased by 18.9%). Meanwhile, the torsional ductility was decreased by 23.9 % and 35.3 % with increased stirrup spacing from 100 mm to 150 mm and 200 mm, respectively. The torsional ductility of SP-100-L-1.50 and SP-100-L-3.00 increased by 24.9% and 36.7%.

The effects of spiral reinforcement states, spiral reinforcement ratio, and the steel fiber content on torsional ductility were essentially equal. Torsional ductility was mainly related to the deformation of RPC beams after the stirrup yielded. The stronger the deformation capacity showed, the better the torsional ductility of RPC beams. As shown in Fig. 9, it is concluded that RPC beam with locked SP had a large deformation after the stirrup yielded due to prominent synergy with longitudinal reinforcement. Therefore, the torsional ductility of RPC beams with locked SP was better than that of RPC beams with equal amount of ordinary stirrup. However, the stirrup was easier to yield and had weaker crack suppression effect with the wide stirrup spacing. So, RPC beams with wider stirrup spacing were more vulnerable and less ductile. The use of steel fiber enhanced the tensile and compressive strength of RPC significantly, suppressed the internal damage of the beam, and avoided the failure of the beam due to concrete damage. Therefore, the increase of steel fiber content reduced the plastic strain of the stirrup, while the torsional ductility of the beam was improved.

4.4. Torsional stiffness

Table 7 illustrates the change in torsional stiffness of RPC beams during loading. The pre-cracking torsional stiffness (K_{cr}) denotes the stiffness of the test beam before cracking. The pre-yielding torsional stiffness (K_y) denotes the stiffness of the test beam after cracking and before yielding of the rebars. The pre-ultimate torsional stiffness (K_u) denotes the stiffness of the test beam after yielding of the rebars until the test beam is failed. For RPC beams without stirrups, the pre-cracking torsional stiffness (K_{cr}) of P and I was greater than that of RPC beams with stirrups, which P was greater than I. This is stated that the presence of steel rebar had a two-sided effect on the K_{cr}. In general, the strength and elastic modulus of the steel bar were much larger than that of the RPC material, which increased the K_{cr} of RPC beams. From the microscopic point of view, the existence of steel bar increased weak interface between steel bar and RPC material, which reduced the torsional stiffness of RPC beams. The increasing weak interface played a dominant role in the change of K_{cr} due to the small forces on rebars before cracking. This results in the less steel bars in RPC beams showed greater the K_{cr}. When the stirrup spacing was identical, the weak interface of RPC beams with SP was less than that of beams with ordinary stirrup, and the SP could more effectively bore the tension after cracking, which limited the deformation. After the stirrup yielded with a larger deformation, the K_u was less affected. Compared with ST-100–0.75, the K_{cr} and K_y of SP-100-L-0.75 were increased by 16.7% and 27.6%. The difference between the K_u of SP-100-L-0.75 and ST-100–0.75 was small.

Similarly, the K_{cr} of RPC beams was almost independent of the locking and unlocking effect of the SP due to the same volume of stirrup. However, locked SP could limit crack development and reduce deformation of RPC beams after cracking. Therefore, the K_y of SP-100-L-0.75 was increased by 22% compared to SP-100-U-0.75. On the contrary, when the spacing of locked SP changed from 100 mm to 150 mm and 200 mm, the K_y of RPC beams distinctly decreased by 32.1% and 63.1%, while the K_{cr} and K_u were approximately the same. This reveals that the K_{cr} and K_u of RPC beams did not varied with the spacing of locked SP, while the K_y dropped significantly, similar as the findings from Calioris [10] and Hadhood [16]. It is caused that the restraining ability of stirrups to torsional deformation and cracks was weak before cracking and after the stirrups yield. The restraint was greater between cracking with stirrups yielding.

When stirrup spacing and torque direction were determined, the K_{cr} , K_y and K_u strengthened with increasing steel fiber content. In addition, the increasing the steel fiber content resulted in larger increase in the K_y, and a smaller increase in the K_u. When the steel fiber content in RPC beams changed from 0.75% to 1.50% and 3.00%, the K_y of RPC beams increased by 55.7% and 98.6%, while the K_u increased by only 10.2%

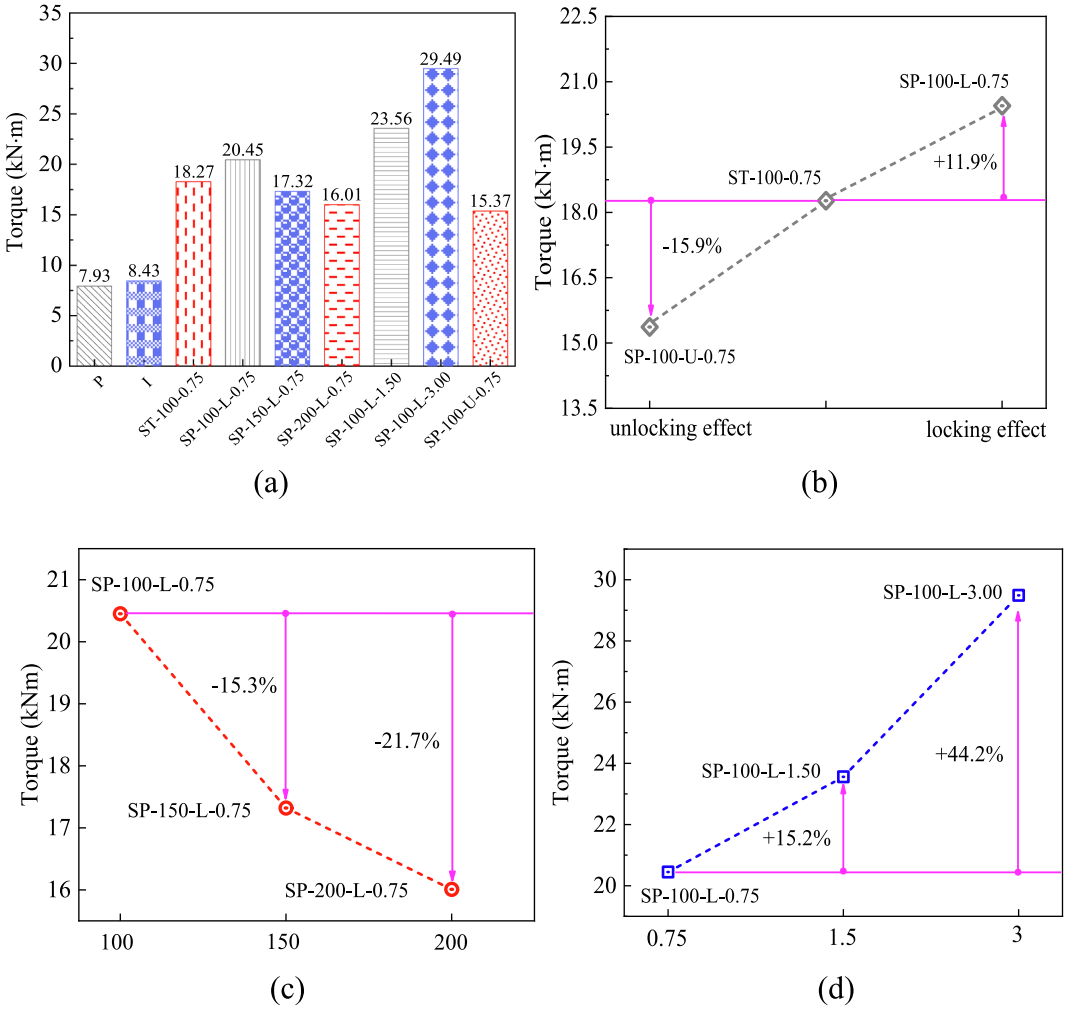

Fig. 11. Effects of test parameters on ultimate torque. (a) ultimate Torque of RPC Beams, (b) effect of spiral reinforcement condition on ultimate torque, (c) effect of spiral reinforcement spacing on ultimate torque, (d) effect of steel fiber content on ultimate torque.

and 18.4%. After cracking, the steel fiber not only limited the crack development, but also heightened the weak interface between the steel bar and the RPC. Therefore, the stiffness was strongly affected by the steel fiber at this stage. After the stirrup yielded, most steel fibers at oblique cracks were pulled out, so the effect of steel fibers on stiffness was limited.

4.5. Energy dissipation

Based on the law of conservation of energy, the energy dissipation of each beam was compared. The energy dissipation calculation model is shown in Fig. 13 [36]. The curve OAB represents torque versus twist curve of tested beams.

$$W = W_E + W_P = S_{OAD} + S_{ABCD} \tag{2}$$

$$S_i = \int_0^{\theta} f(x)\mathrm{d}x \tag{3}$$

where W is the total energy dissipation of tested beam; W_E is the elastic deformation energy dissipation; W_P is the plastic deformation energy dissipation; S_{OAD} is the area of the region OAD; W_{ABCD} is the area of the region ABCD; $f(x)$ is the equation of measured torque versus twist curve.

Table 8 summarizes the actual energy dissipation of all RPC beams. There was only elastic energy dissipation for P and I, which had fine distinction. The energy dissipation of RPC beams without stirrups was less affected by longitudinal reinforcement. It also is observed that the total energy dissipation of RPC beams with SP was significantly preferred than that of RPC beams without stirrups. In addition, plastic energy dissipation accounted for about 95% of the total energy dissipation, which was significantly larger than elastic energy dissipation. This indicates that the energy dissipation of RPC beams was associated with steel rebar. The greater the deformation of steel rebar accompanied by more energy dissipation under the same conditions. The steel deformation of SP-100-L-0.75 was more than ST-100–0.75, and its energy dissipation was increased by 30.5% with same stirrup spacing. While the SP was unlocked, the deformation ability of steel bar could not be fully utilized. The energy dissipation of SP-100-U-0.75 was 67.4% lower than that of SP-100-L-0.75. However, the number of stirrups and the force of longitudinal reinforcement force decreased with the increase of stirrup spacing, resulting in weakening overall deformation of steel rebar. The decline in the energy dissipation of SP-150-L-0.7 and SP-200-L-0.75 was 38.5% and 48.4% of the energy dissipation of SP-100-L-0.75. Similar to torsional ductility and torsional stiffness, the energy dissipation also tended to increase with the increase of steel fibers. The mechanism of energy dissipation was also the same as that of the torsional ductility and torsional stiffness development law mechanism.

5. Ultimate torque calculation method

For the calculation method of ultimate torque, the softened space

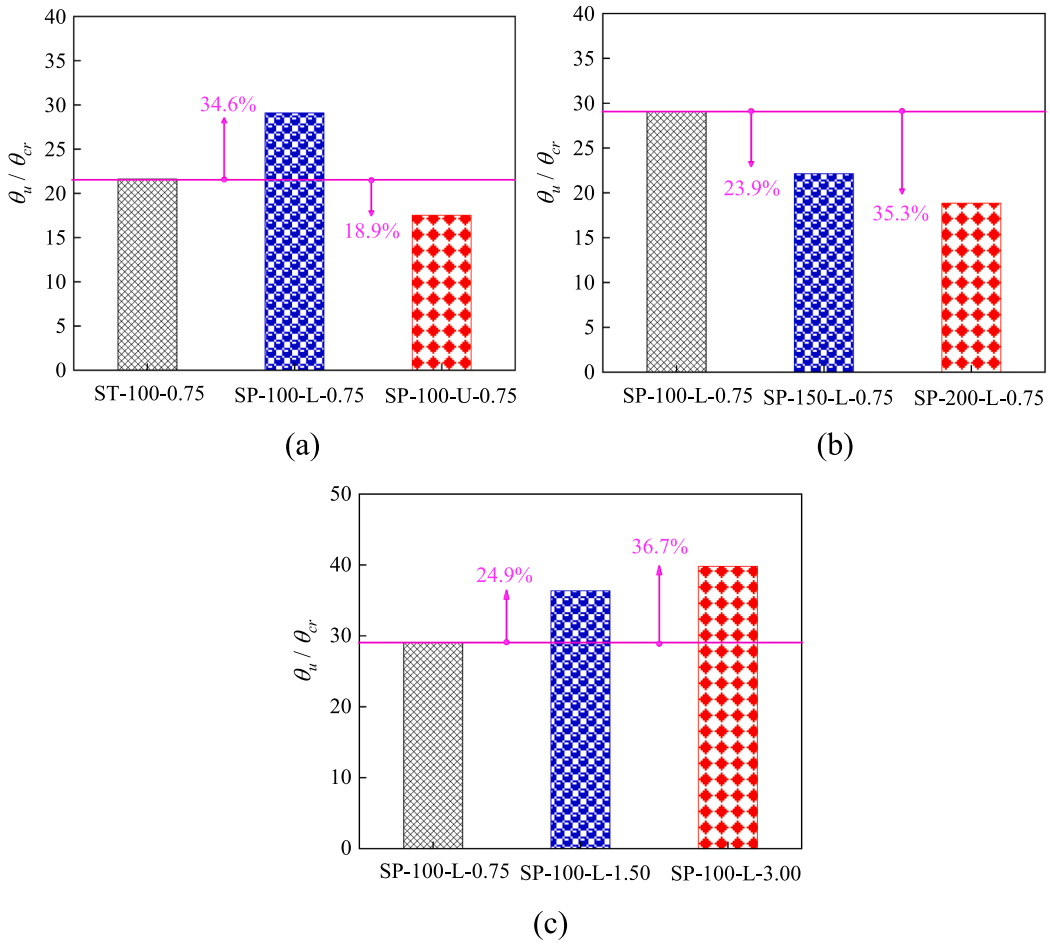

Fig. 12. Effects of test parameters on torsional ductility. (a) effect of spiral reinforcement condition on torsional ductility, (b) effect of spiral reinforcement spacing on torsional ductility, (c) effect of steel fiber content on torsional ductility.

Table 7
Torsional stiffness of RPC beams.

Group	Test beam	K_{cr}(kN·m²/rad)	K_y(kN·m²/rad)	K_u(kN·m²/rad)
Control	P	3448	—	—
	I	3128	—	—
Lock and unlock effects of the SP	ST-100–0.75	2506	225	139
	SP-100-L-0.75	2924	287	147
	SP-100-U-0.75	3223	235	228
stirrup spacing of the SP	SP-100-L-0.75	2924	287	147
	SP-150-L-0.75	3148	195	154
	SP-200-L-0.75	2940	106	157
Steel fiber content	SP-100-L-0.75	2924	287	147
	SP-100-L-1.50	3684	447	162
	SP-100-L-3.00	4676	570	174

Where $K_{cr} = \frac{T_{cr}}{\theta_{cr}}$, $K_y = \frac{T_y - T_{cr}}{\theta_y - \theta_{cr}}$, $K_u = \frac{T_u - T_y}{\theta_u - \theta_y}$.

truss model [37] had been recognized by many scholars. The model considered the longitudinal reinforcement, the stirrup, and the concrete with oblique cracks as forming a space truss to bore the torque. Calioris [10] proposed a new ultimate torque calculation model based on the softened space truss model, considering the influence of the inclination angle of the SP on the ultimate torque. However, the ultimate torque calculation formula based on the SP ignored the contribution of concrete tensile strength and steel fibers for the ultimate torque. It was clear from the experimental results in this study that the ultimate torque of RPC beams was influenced by the steel fibers and concrete tensile strength. The ultimate torque calculation formula proposed by Calioris was not applicable to RPC beams. From the experimental results, the steel strain was minor before cracking and the torque was mainly borne by RPC. Therefore, the ultimate torque of the RPC beams was considered as consisting of the torque borne by steel rebar (T_S) and the torque borne by concrete (T_C). In this paper, the torsional effects of concrete tensile strength and steel fibers were considered and the formula for calculating the ultimate torque of RPC beams was proposed on the basis of Calioris.

5.1. Ultimate torque calculation model

5.1.1. Consideration of the impact of steel fibers on ultimate torque

In order to analyze the contribution of steel fibers to the ultimate torque of RPC beams, steel fibers were equivalent to the steel fiber spiral reinforcement, as shown in Fig. 14. Meanwhile, steel fibers should meet two basic assumptions: (1) the sum of adhesion stress between all steel fibers and RPC was equal to the sum of the effective forces provided by all equivalent steel fiber stirrup; (2) There was no interaction force between equivalent steel fiber stirrups.

The total volume V_f of steel fibers in RPC beam was divided into n steel fiber equivalent stirrups with cross-sectional area A_{SF}.

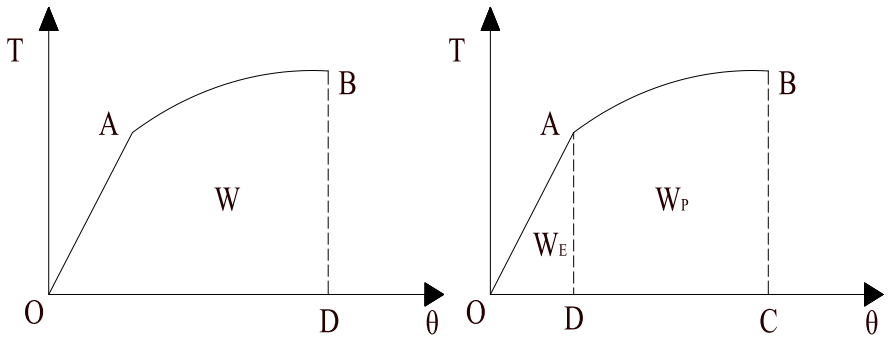

Fig. 13. Energy consumption calculation method.

Table 8
Energy dissipation of RPC beams.

Group	Test beams	W_E(kN·m²)	W_P(kN·m²)	W(kN·m²)
Control	P	0.009	—	0.009
	I	0.015	—	0.015
Lock and unlock effects of the SP	ST-100–0.75	0.028	1.033	1.061
	SP-100-L-0.75	0.032	1.353	1.385
	SP-100-U-0.75	0.019	0.432	0.451
Stirrup spacing of the SP	SP-100-L-0.75	0.032	1.353	1.385
	SP-150-L-0.75	0.022	0.83	0.852
	SP-200-L-0.75	0.025	0.69	0.715
Steel fiber content	SP-100-L-0.75	0.032	1.353	1.385
	SP-100-L-1.50	0.042	1.749	1.791
	SP-100-L-3.00	0.052	2.236	2.288

WhereW_E = the elastic deformation energy dissipation, W_P= the plastic deformation energy dissipation, W= the total energy dissipation.

The formula for calculating the cross-sectional area A_{SF} of the equivalent stirrup was as follows:

$$A_{SF} = \frac{V_f}{2(b_0+h_0)n} = \frac{\rho_f L_1 bh}{2(b_0+h_0)(L_1/S+1)} \tag{4}$$

where ρ_f is the volume ratio of steel fiber; L_1 is the length of the pure torsion test region of RPC beam;b and h are the width and height of RPC beam;b_0 and h_0 are the width and height of the area enclosed by the centerline of the stirrup;S is the stirrup spacing of tested beam.

The steel fibers were pulled out when the test beam failed. But it is difficult to measure the tensile stress between RPC and each steel fiber after RPC beam cracking. For the convenience of calculations, shear stress between the fiber and the RPC matrix was regarded as the strength of equivalent steel fiber stirrup (f_{SF}). Due to the lack of test data for RPC, the calculation formula of steel fiber reinforced concrete (SFRC) was adopted. When RPC beams were used in flat type steel fibers, the f_{SF} was calculated based on the equation suggested in Singh [38] as follows:

$$f_{SF} = 0.75\sqrt{f_{cu}} \tag{5}$$

where f_{cu} is the compressive strength of RPC.

5.1.2. Contribution of steel rebar to ultimate torque (T_S)

Under the influence of the torque, shear flow was formed in the cross-section of RPC, as shown in Fig. 15. q is calculated in Eq. (6).

$$q = \frac{T_S}{2A_0} \tag{6}$$

When the SP was locked, the force direction of equivalent steel fiber stirrup and SP was consistent, as shown in Fig. 15 (b). Force equilibrium along two axes leaded to two equations, respectively:

$$qp_0 = (F_{LR} + F_{TR}\cos\varphi_{front} + F_{SF}\cos\varphi_{front})\tan\theta \tag{7}$$

$$qS = (F_{TR}\sin\varphi_{front} + F_{SF}\sin\varphi_{front})\cot\theta \tag{8}$$

Substituting Eq (5) into Eq (6), the ultimate torque based on longitudinal axis was established:

$$T_L = \frac{2\left(F_{LR} + F_{TR}\cos\varphi_{front} + F_{SF}\cos\varphi_{front}\right)A_0}{p_0}\tan a \tag{8.a}$$

Substituting Eq (5) into Eq (7), the ultimate torque based on transverse axis was established:

$$T_T = \frac{2\left(F_{TR}\sin\varphi_{front} + F_{SF}\sin\varphi_{front}\right)A_0}{S}\cot a \tag{8.b}$$

Combining Eq (8.a) and Eq (8.b), the cracking angle,a is deduced:

$$\tan a = \sqrt{\frac{\left(F_{TR}\sin\varphi_{front} + F_{SF}\sin\varphi_{front}\right)p_0}{\left(F_{LR} + F_{TR}\cos\varphi_{front} + F_{SF}\cos\varphi_{front}\right)S}} \tag{9}$$

Where $F_{LR} = A_{LR}f_{LR}$;$F_{TR} = A_{TR}f_{TR}$;$F_{TR} = A_{TR}f_{TR}$; A_{LR} is the cross-sectional area of all longitudinal reinforcements; f_{LR} is the yield strength of the longitudinal reinforcement; A_{TR} is the cross-sectional

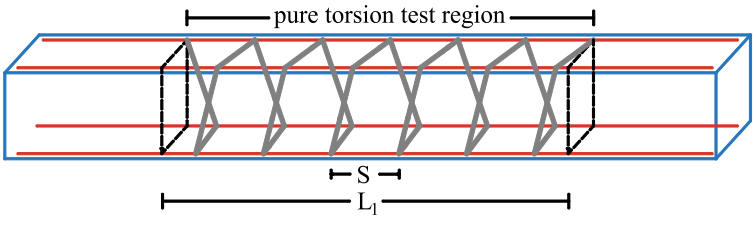

Fig. 14. Steel fiber equivalent spiral reinforcement.

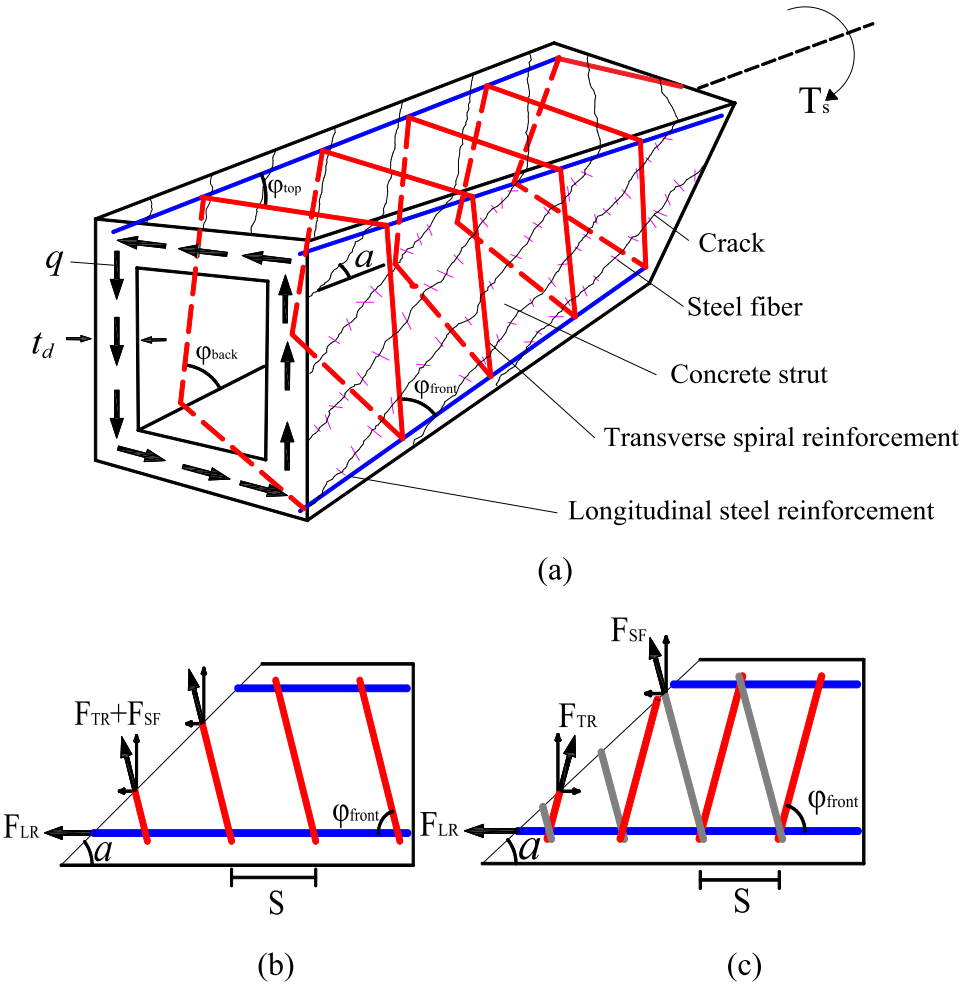

Fig. 15. Simplified torsional analysis based on the space truss theory, (a) space truss components of a RC beam under pure torsion, (b)SP with locking effect, (c)SP with unlocking effect,

area of single transverse reinforcement; f_{TR} is the yield strength of the transverse reinforcement; p_0 is the perimeter of the shear flow centerline; A_0 is the of the area of the shear flow centerline, as follow Eq. (10); S is the stirrup spacing.

$$A_0 = 0.85\left(\frac{h_0}{\sin\varphi_{front}} \times \frac{b_0}{\sin\varphi_{top}}\right) \tag{10}$$

where b_0 and h_0 are the width and height of the area enclosed by the centerline of SP, respectively; φ_{fornt} and φ_{top} are the inclination angles of the side and top of SP, respectively [16].

When the SP was unlocked, the force direction of equivalent steel fiber stirrup and SP is opposite, as shown in Fig. 15 (c). Force equilibrium along two axes leaded to two equations, respectively:

$$qp_0 = (F_{LR} - F_{TR}\cos\varphi_{front} + F_{SF}\cos\varphi_{front})tan\theta \tag{11}$$

$$qS = (F_{TR}\sin\varphi_{front} - F_{SF}\sin\varphi_{front})\cot\theta \tag{12}$$

Likewise, substituting Eq (5) into Eq. (11) and Eq. (12), the ultimate torque based on longitudinal and transverse axis was established, respectively:

$$T_X = \frac{2\left(F_{LR} - F_{TR}\cos\varphi_{front} + F_{SF}\cos\varphi_{front}\right)A_0}{p_0}\tan a \tag{13.a}$$

$$T_Y = \frac{2\left(F_{TR}\sin\varphi_{front} - F_{SF}\sin\varphi_{front}\right)A_0}{S}\cot a \tag{13.b}$$

Combining Eq. (13.a) and Eq. (13.b), the cracking angle,a is deduced:

$$\tan a = \sqrt{\frac{\left(F_{TR}\sin\varphi_{front} - F_{SF}\sin\varphi_{front}\right)p_0}{\left(F_{LR} - F_{TR}\cos\varphi_{front} + F_{SF}\cos\varphi_{front}\right)S}} \tag{14}$$

Eq. (8) and (13) simplify the consideration of the effect of spiral reinforcement and steel fibers on the torque, respectively, which were used for the calculation of the torque of steel rebar (T_S) in RPC beams with SP. Meanwhile, when φ_{front} and φ_{top} were equal to 90°, the formulas were used to calculate the torque of steel rebar (T_S) in RPC beams with ordinary stirrups. There was no steel fiber in the beam, it also was better connected with the calculation of torque in previous studies [10].

5.1.3. Contribution of concrete to ultimate torque (T_C)

The rectangular beam is idealized as a thinwalled tube with a thickness of t_d. The force sketch of the concrete under the torque (T_C) is illustrated in Fig. 16. Force equilibrium along longitudinal axis:

$$f_{te}t_d h_0\cos\theta\cot\theta = \frac{T_C}{2A_0}h_0 \tag{15}$$

Substituting $q = \frac{T_C}{2A_0}$ into Eq. (15), it was converted:

$$T_C = 2f_{te}t_d A_0\cos a\cot a \tag{16}$$

where t_d is the effective wall thickness; f_{te} is the main tensile stress of RPC when the beam is cracked, Based on Li's study, f_{te} is taken as $0.671f_{t,m}$ based on Li's study[39].

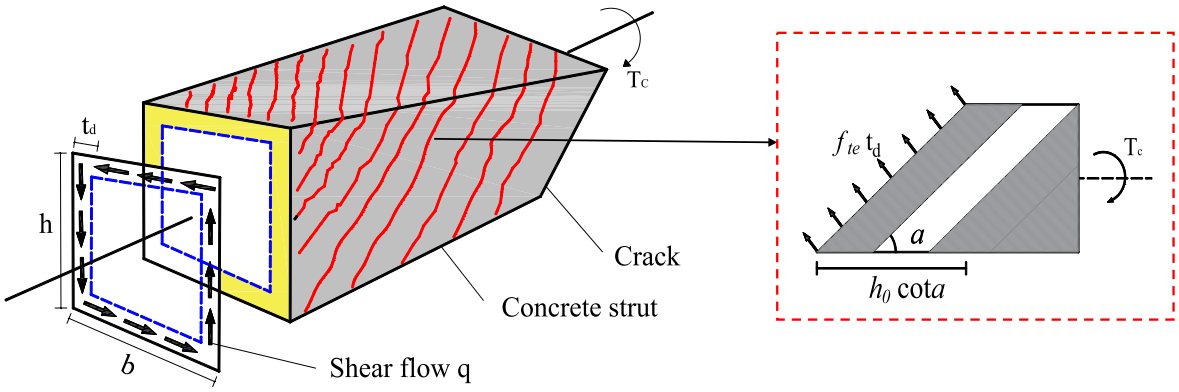

Fig. 16. Analysis of cross-sections of specimens under pure torsion.

Combining Eq. (8), Eq. (13) and Eq. (16), the ultimate torque of RPC beam was calculated as:

$$T_u = T_S + T_C = \min\{T_{SX}, T_{SY}\} + T_C \tag{17}$$

5.2. Comparisons of analytical and experimental results

In order to verify the calculation accuracy of the proposed formula, the experimental data and the calculated data of the formula were compared and analyzed. The experimental data included seven RPC beams from this paper and fourteen beams from previous studies [23–24].The experimental results (T_{exp}) and calculation results (T_{cal}) for all RPC beams are listed in Table 9, and the correlation between the T_{exp} and T_{cal} is depicted in Fig. 17. The average, variance, and coefficient of variation of the ratio of tested and calculated values are 1.05, 0.17 and 0.16, respectively. It is indicated that the formula proposed in this paper can predict the ultimate torque of RPC beams accurately. The formular accuracy of ultimate torque for RPC beams is improved on the basis of considering concrete tensile strength and steel fiber. However, the torsional test data of RPC beams are relatively scarce, and more test data are needed to further verify formula in this study.

6. Conclusions

Nine RPC beams were subjected to torque was investigated, the difference in torsional performance of RPC beams between ordinary stirrup and spiral reinforcement (SP). This study further analyzed the effect of different parameter, including spiral reinforcement configuration, spiral reinforcement ratio, and the steel fiber content, on the torsional performance of RPC beams with SP, following conclusions were demonstrated.

Table 9
The experimental results and calculation results for all RPC beams.

Data source	specimens	T_{cal}	T_{exp}	T_{exp}/T_{cal}
This study	ST-100–0.75	19.00	18.27	0.96
	SP-100-L-0.75	19.60	20.45	1.04
	SP-150-L-0.75	18.25	17.32	0.95
	SP-200-L-0.75	18.12	16.01	0.88
	SP-100-L-1.50	21.53	23.56	1.09
	SP-100-L-3.00	22.63	29.49	1.3
	SP-100-U-0.75	18.94	15.37	0.81
Yang et al.[23]	SS-F1-L56-S35	74.66	75.30	1.01
	SS-F1-L56-S70	66.91	86.70	1.3
	SS-F2-L56-S35	114.05	85.60	0.75
	SS-F2-L56-S70	82.49	109.80	1.33
	SS-F2-L88-S35	117.18	114.70	0.98
	SS-F2-L88-S70	100.47	115.20	1.15
	SS-F2-L127-S35	146.41	109.60	0.75
	SS-F2-L127-S70	125.63	119.30	0.95
Zhou et al[24]	HB200T50-1	21.97	19.55	0.89
	HB200T50-2	21.97	21.12	0.96
	HB300T50-1	43.08	44.22	1.03
	HB300T50-2	43.08	46.63	1.08
	HB300T80-2	52.66	64.11	1.22
	HB300T80-2	52.66	61.47	1.17
	CHB300T50-1	48.53	62.27	1.28
	CHB300T50-2	48.53	63.36	1.31

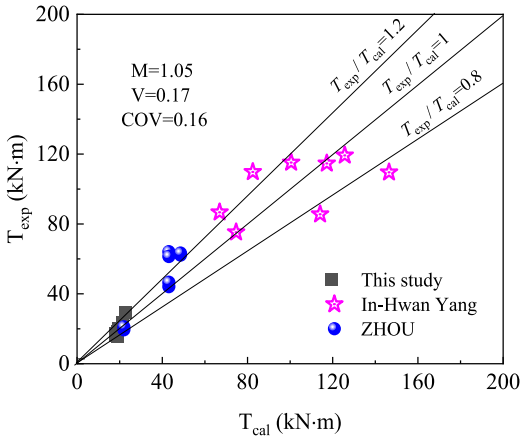

Fig. 17. The correlation between T_{exp} and T_{cal}.

(1). The synergy of steel rebar, stress redistribution, crack suppression and torsional deformation of RPC beams with locked SP were better than RPC beams with ordinary stirrups, while the various torsional performances of RPC beams with unlocked SP were inferior to RPC beams with ordinary stirrups. The ductility, energy dissipation and ultimate torque of RPC beams with locked SP were improved by 13.7%, 30.5%, 11.9% compared to RPC beams with ordinary stirrup. The RPC beam with unlocked SP was weaker by 26.5%, 57.5%, 15.9% than RPC beam with ordinary stirrups.

(2). The torsional ductility, energy dissipation and ultimate torque of RPC beams with locked SP were reduced with the increase of stirrup spacing and enhanced with the increase of steel fiber content. The maximum decrease of torsional ductility, energy dissipation and ultimate torque was 38.2%, 48.4%,21.7% with the increase of stirrup spacing, respectively. The maximum increment of torsional ductility, energy dissipation and ultimate torque was 32.5%, 65.2%, 44.2% with the increase of steel fiber content, respectively. The effect of stirrup spacing on the torsional ductility of RPC beams with locked SP was higher than the steel fibers, and the effect on the energy dissipation and ultimate torque of RPC beams was lower than the steel fibers.

(3). When the stirrup was changed from normal stirrup to the SP, the pre-cracking torsional stiffness and pre-yielding torsional stiffness of RPC beams with SP were increased and the pre-ultimate torsional stiffness was basically the same. The increase of stirrup spacing had a negative effect on the pre-yielding torsional stiffness, while had no effect on the pre-cracking torsional stiffness and pre-ultimate torsional stiffness. In contrast to the stirrup spacing, increasing steel fiber content had favorable effect on three types of torsional stiffness.

(4). The cracking torque of the RPC beam was not affected by the unlocking and locking effect of the SP. RPC beams with stirrup spacing of 150 mm and 200 mm produced descending cracking torque compared to beam with stirrup spacing of 100 mm. The addition of steel fiber significantly improved the cracking torque of RPC beams with locked SP.

(5). Considering the RPC tensile strength and steel fibers in the ultimate torque equation minished the deviation and dispersion degree between the calculation results and the test results. Therefore, the ultimate torque calculation formula proposed in this study for RPC beams with stirrup was admissible. However, there are few studies on RPC beams subjected to torsion, and more experimental data were needed to verify further formula.

CRediT authorship contribution statement

Xia Cao: Conceptualization, Investigation, Methodology, Supervision. **Yong-peng Quan:** Investigation, Writing – review & editing. **Yi-cheng Ren:** Investigation, Writing – review & editing. **Feng Fu:** Investigation, Writing – review & editing. **Qi-zhi Jin:** Supervision. **Da-bo He:** Writing – review & editing. **Yan Zheng:** Supervision.

Declaration of Competing Interest

The authors declare that they have no known competing financial interests or personal relationships that could have appeared to influence the work reported in this paper.

Data availability

Data will be made available on request.

Acknowledgments

This research was supported by the National Nature Science Foundation of China (No. 52068012, 51968013, 52168068), Guangxi Key Laboratory of Green Building Materials and Construction Industrialization (No. 19-J-21-6) and Guangxi University young and middle-aged teachers basic ability improvement project (No. 2019KY0267). Natrual Science Foundation of Guangxi,(No.2022GXNSFAA035529). Any opinions, findings and conclusions expressed in this paper do not necessarily reflect the view of the sponsors.

Data availability

Some or all data, models, or code that support the findings of this study are available from the corresponding author upon reasonable request.

References

[1] Lee HS, Hwang KR. Torsion design implications from shake-table responses of an RC low-rise building model having irregularities at the ground story. Earthquake Engng Struct Dyn 2015;44:907–27.
[2] Mondal TG, Prakash SS. Nonlinear finite-element analysis of RC bridge columns under torsion with and without axial compression. J Bridge Eng 2016;21(2):0401503.
[3] Eom TS, Kang SM, Park HG, et al. Cyclic loading test for reinforced concrete columns with continuous rectangular and polygonal hoops. Eng Struct 2014;67:39–49.
[4] Karayannis CG, Chalioris CE. Shear tests of reinforced concrete beams with continuous rectangular spiral reinforcement. Construct Build Mater 2013;46:86–97.
[5] Corte WD, Boel V. Effectiveness of spirally shaped stirrups in reinforced concrete beams. Eng Struct 2013;52:667–75.
[6] Azimi M, Campos UA, Matthews JC, et al. Experimental and numerical study on cyclic performance of reinforced concrete exterior connections with rectangular spiral reinforcement. J Struct Eng 2020;146(3):04019219.
[7] Saha P, Meesaraganda VP. Experimental investigation of reinforced SCC beam-column joint with rectangular spiral reinforcement under cyclic loading. Construct Build Mater 2019;201:171–85.
[8] Fan G, Zhao Z, Yang G. Cyclic response of reinforced concrete shear walls with continuous rectangular spiral stirrups. KSCE J Civ Eng 2018;22(5):1771–81.
[9] Shatarat N, Hunifat R, Murad Y, et al. Torsional capacity investigation of reinforced concrete beams with different configurations of welded and unwelded transverse reinforcement. Struct Concr 2020;21:484–500.
[10] Chalioris CE, Karayannis CG. Experimental investigation of RC beams with rectangular spiral reinforcement in torsion. Eng Struct 2013;56(6):286–97.
[11] Ibrahim A, Askar HS, El-Zoughiby ME. Torsional behavior of solid and hollow concrete beams reinforced with inclined spirals. J King Saud Univ Sci 2020.
[12] Shahrooz BM, Forry ML, Anderson NS, et al. Continuous transverse reinforcement-behavior and design implications. ACI Struct J 2016;113(5):1085–94.
[13] Prakash S, Belarbi A, You YM. Seismic performance of circular RC columns subjected to axial force, bending, and torsion with low and moderate shear. Eng Struct 2010;32(1):46–59.
[14] Wang P, Han Q, Du X. Seismic performance of circular RC bridge columns with flexure–torsion interaction. Soil Dyn Earthq Eng 2014;66:13–30.
[15] Askandar NH, Mahmood AD. Torsional strengthening of RC beams with continuous spiral near-surface mounted steel wire rope. Int J Concr Struct M 2020;14(1):1–16.
[16] Hadhood A, Gouda MG, Agamy MH, et al. Torsion in concrete beams reinforced with GFRP spirals. Eng Struct 2020;206:110174.
[17] Yalciner H, Kumbasaroglu A, Turan AI. Torsional behavior of reinforced concrete beams with corroded reinforcement. Structures 2019;20:476–88.
[18] Mohamed HM, Benmokrane B. Reinforced concrete beams with and without FRP web reinforcement under pure torsion. J Bridge Eng 2016;21(3):04015070.
[19] Lopes SMR, Bernardo LFA. Cracking and failure mode in HSC hollow beams under torsion. Construct Build Mater 2014;51:163–78.
[20] Sha H, Liu J. Static mechanical properties of reactive powder concrete reinforced with basalt fibers. Struct Concr 2022;23(3):1675–86.
[21] Ahmed S, Al-Dawood Z, Abed F, et al. Impact of using different materials, curing regimes, and mixing procedures on compressive strength of reactive powder concrete - a review. J Build Eng 2021;7:103238.
[22] Khuzaie HA, Atea RS. Investigation of torsional behavior and capacity of reactive powder concrete (RPC) of hollow T-beam. J Mater Res Technol 2019;8(1):199–207.
[23] Yang IH, Joh C, Lee JW, et al. Torsional behavior of ultra-high performance concrete squared beams. Eng Struct 2013;56:372–83.
[24] Zhou JL, Li CX, Feng Z, et al. Experimental investigation on torsional behaviors of ultra-high-performance fiber-reinforced concrete hollow beams. Cem Concr Compos 2022;129:104504.
[25] Kwahk I, Joh C, Lee JW. Torsional behavior design of UHPC box beams based on thin-walled tube theory. Engineering 2015;07(3):101–14.
[26] Cao X, Ren YC, Zhang L, et al. Flexural behavior of ultra-high-performance concrete beams with various types of rebar. Compos Struct 2022;292:115674.
[27] Cao X, Ren YC, Qian K, et al. Size effect on flexural behavior of ultra-high-performance concrete beams with different reinforcement. Structures 2022;41:969–81.
[28] ACI 318-14, Building Code Requirements for Structural Concrete and Commentary, Farmington Hills, American Concrete Institute Committee, 2014.
[29] Deifalla A, Ghobarah A. Behavior and analysis of inverted T-shaped RC beams under shear and torsion. Eng Struct 2014;68:57–70.
[30] Zhou J, Chen ZP, Chen YL, et al. Torsional behavior of steel reinforced concrete beam with welded studs: experimental investigation. J Build Eng 2022;48:103879.
[31] Chalioris CE. Experimental study of the torsion of reinforced concrete members. Struct Eng Mech 2006;23(6):713–37.
[32] Rao T, Seshu DR. Torsion of steel fiber reinforced concrete members. Cem Concr Res 2003;33(11):1783–8.
[33] Bernardo LFA, Teixeira MM. Modified softened truss-model for prestressed concrete beams under torsion. J Build Eng 2018;19:49–61.
[34] Zhou C, Wang J, Jia W, et al. Torsional behavior of ultra-high performance concrete (UHPC) rectangular beams without steel reinforcement: experimental investigation and theoretical analysis. Compos Struct 2022;299:116022.
[35] Chalioris CE, Karayannis CG. Effectiveness of the use of steel fibres on the torsional behaviour of flanged concrete beams. Cem Concr Compos 2009;31(5):331–41.
[36] Chen LY, Zhong M, Chen ZP. Pure torsional experiment and damage analysis of welded stud steel reinforced concrete beams. Build Struct 2019;4:9.
[37] Hsu T. Unified theory of reinforced concrete-A summary[M]. CRC Press; 1993.
[38] Singh H. Flexural modeling of steel fiber-reinforced concrete members: analytical investigations. Pract Period Struct Des Constr 2014;20(4):04014046.
[39] Cx LI, Zhou JL, Ke L, et al. Experimental investigation and calculation of the torsional capacity of reinforced UHPC rectangle beams. Chin J Hwy Trans 2021;34(08):118–31.

[40] Fu F, Parke GAR. Assessment of the progressive collapse resistance of double-layer grid space structures using implicit and explicit methods. Int. J. Steel Struct. 2018; 18(3):831–42.
[41] Qian K, Weng Y-H, Fu F, Deng X-F. Numerical evaluation of the reliability of using single-story substructures to study progressive collapse behaviour of multi-story RC frames. J. Build. Eng. 2021;33:101636.
[42] Qian K, Lan DQ, Fu F, Li B. Effects of infilled wall opening on load resisting capacity of RC frames to mitigate progressive collapse risk. Eng. Struct. 2020;223: 111196.